Int J Heat Mass Transfer Vol 33, No 11, pp 2491–2502, 1990
Printed in Great Britain

0017–9310/90 $3 00+0 00

The application of an embedded grid to the solution of heat and momentum transfer for spheres in a linear array

J S TSAI and ARTHUR M STERLING

Department of Chemical Engineering, Louisiana State University, Baton Rouge, LA 70803, U.S A

(*Received* 15 *June* 1989 *and in final form* 27 *December* 1989)

Abstract—The objective of this study is to predict the forced convection heat transfer for spheres in a one-dimensional array aligned along the flow direction An array with spheres of different sizes has also been studied The interaction among these spheres is a salient feature of the analysis The Navier–Stokes equations, in pressure–velocity form, and the energy equation have been solved numerically by an iterative finite-difference method in an embedded, body-fitted grid A range of Reynolds numbers from 5 to 100 has been investigated for two sphere spacings. The temperature distribution around the sphere array, as well as the drag coefficient and Nusselt number around the sphere surfaces have been calculated The results show good agreement with the numerical and experimental results in the literature

INTRODUCTION

FUEL DROPLET combustion has received considerable attention in recent years Most theoretical work has focused on the combustion of a single, isolated droplet or on the group combustion behavior of sprays It has been recognized, however, that in any spray combustion process, droplet–droplet interactions reduce the gasification rate of participating droplets. Hence it is necessary to gain a better understanding of these phenomena to improve our ability to predict the combustion behavior of fuel sprays

A few theoretical approaches, based on an assumption of potential flow, have been proposed to model interacting droplet arrays For two-droplet systems, bipolar coordinates were used by Umemura *et al.* [1] to describe the interaction between droplet pairs. For various multi-droplet arrays, Labowsky [2] proposed a technique, based on the method of images, to calculate the burning rate of each individual droplet in an array All of the above calculations were performed for droplet arrays burning in a quiescent, oxidizing atmosphere, i e. for diffusion controlled transfer processes

In a real combustor, however, forced convection may dominate the transfer processes, and combustion conditions may differ considerably from those in a quiescent environment Thus a diffusion-limited analysis is inadequate and the convective effects need to be taken into account. In particular, the effect of forced convection on droplet–droplet interactions depends both on the relative arrangement of spheres in an array and on the orientation of the array with respect to the flow direction

Shuen [3] studied the combustion of a planar droplet array oriented normal to the approaching flow and concluded that the interaction decreases as the Reynolds number increases. In contrast, for arrays with droplets aligned in tandem along the flow direction, Aminzadeh *et al.* [4], Chen and Tong [5], and Tal *et al.* [6, 7] found that the interaction increases as the Peclet number or Reynolds number increases.

The linear droplet array, although an approximation of a dense spray system, provides a convenient system for the study of some key factors dominating the spray combustion process, such as the effects of Reynolds number, droplet–droplet spacing, and droplet size on the heat and mass transfer behavior of the participant droplets In contrast to the single droplet case, which provides an upper limit for convective heat and mass transfer rates in the absence of droplet–droplet interactions, a linear array of droplets aligned with the flow allows for a maximum interaction between droplets Thus the asymptotic behavior observed for downstream droplets will provide a corresponding lower limit for the heat and mass transfer rates. The behavior for droplets in a real, dense spray should fall between these two limits An appreciation of this lower limit will allow improved, conservative engineering models of the complex spray process to be developed

Another important characteristic of real sprays is the droplet size distribution. Clearly, the interaction between two or more droplets of different sizes needs to be described The size differences, however, are neglected in most existing theoretical models because of the increased geometric complexity. Umemura *et al* [1] studied the combustion of pairs of droplets of different sizes in a quiescent environment and concluded that, for any separation of the two droplets, the smaller droplet is affected by the interaction to a greater degree than the larger droplet

In the present analysis, one-dimensional sphere arrays similar to those treated by Chen and Tong [5]

NOMENCLATURE

A coefficient in the general finite-difference equations
C_d total drag coefficient
C_{df} friction drag coefficient
C_{dp} pressure drag coefficient
C_p heat capacity
G convective term normal to grid cell boundary
h non-dimensional enthalpy
J Jacobian of transformation
k thermal conductivity
L distance between the centers of two spheres
Nu Nusselt number
p non-dimensional pressure
Pe Peclet number
Pr Prandtl number
R radius of droplets
Re Reynolds number
S source term in the finite-difference equation for general variables ϕ
T non-dimensional temperature
u, v non-dimensional x and y component of velocities
v_r, v_θ non-dimensional r and θ component of velocities in spherical coordinates
x, y axial and radial coordinates

Greek symbols
α, β, γ coordinate transformation parameter non-dimensional natural coordinates
Γ effective diffusivity for general variable ϕ
$\delta\xi, \delta\eta$ finite-difference mesh spacing in ξ- and η-direction in the transformed plane
$\Delta\xi, \Delta\eta$ cell boundary sizes in ξ- and η-directions in the transformed plane
θ angle from stagnation point
μ non-dimensional viscosity
ρ non-dimensional density
τ surface shear stress
ϕ general variable

Superscripts
$\bar{}$ averaged quantity
$'$ dimensional quality
u u component
v v component

Subscripts
e, w, n, s control volume faces surrounding point p
E, W, N, S neighboring points surrounding point p
f film condition
r radial coordinate in spherical geometry
s sphere surface
θ angular coordinate in spherical geometry
ϕ angle around the symmetric axis
∞ free stream value

and Tal *et al* [6] are studied with the intention of providing additional insight into the spray combustion process. In order to isolate the effect of inter-sphere spacing on the sphere–sphere interaction, the spheres are equally spaced although this restriction can be easily relaxed in the present computational scheme. Furthermore, since the analysis is formulated as a pseudo-steady process, the temporal variation of droplet spacing, owing to non-uniform droplet drag, is not taken into account

A multisphere cylindrical cell, as shown in Fig 1, is used for the calculation domain, and an embedded grid, as shown in Fig 2, fills the interior of the cell. The embedded grid used here eliminates both an inaccuracy and numerical complications introduced by the grid used by Tal *et al* [6] and Chen and Tong [5]. For example, around the sphere surface, a spherical grid is used in the embedded grid and the size of the grid around the sphere surface can be adjusted to a very fine degree without increasing the number of nodes. This not only can provide a more accurate evaluation of the Nusselt number on the sphere surface, but also helps to resolve any steep temperature gradients occurring in the vicinity of the droplet surface, this feature is especially attractive in droplet combustion studies. Another advantage, although not so obvious in this analysis, is important in the study of transient droplet evaporation, where the droplet shrinks as time progresses. At each time step, the entire domain used in refs. [5, 6] needs to be regridded. In the embedded grid used here however, only the spherical grid needs to be regridded, and this is indeed relatively easier and more economical

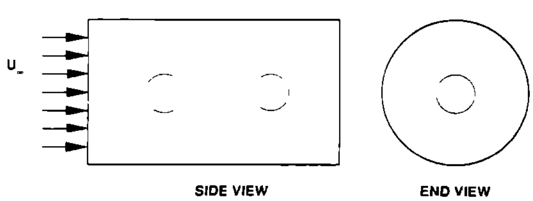

FIG 1 Geometry of the multisphere cylindrical cell

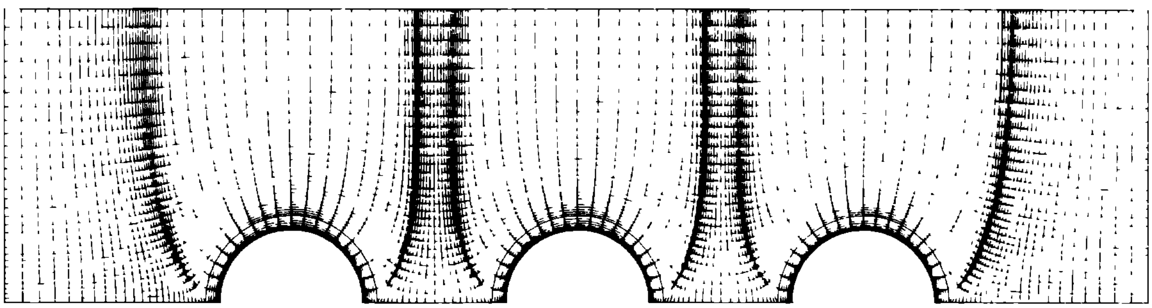

FIG 2 Embedded grid for the present numerical study

The Navier–Stokes equations and the energy equation are solved numerically by an iterative, finite-difference method To better simulate the flow around spheres, variable gas properties are also included in the analysis. Numerical results are obtained for Reynolds numbers from 5 to 100 and two sphere spacings, 4 and 8 sphere radii, respectively. While there is no theoretical limit to the number of tandem spheres that can be included in this model, our present constraints of computer time and storage have precluded the study of more than three spheres

MATHEMATICAL FORMULATION

The linear sphere array in the present analysis is confined in a multisphere cylindrical cell, as shown in Fig. 1 For axisymmetric flow, the conservation equations for mass, momentum, and energy in cylindrical coordinates reduce to those given below

The continuity equation

$$\frac{\partial}{\partial x}(y\rho u)+\frac{\partial}{\partial y}(y\rho v)=0 \tag{1}$$

The momentum equations

x-Component

$$\frac{\partial}{\partial x}(y\rho uu)+\frac{\partial}{\partial y}(y\rho uv) = -y\frac{\partial p}{\partial x} + \frac{2}{Re_\infty}\left[y\frac{\partial \tau_{xx}}{\partial x}+\frac{\partial(y\tau_{xy})}{\partial y}\right]. \tag{2}$$

y-Component

$$\frac{\partial}{\partial x}(y\rho uv)+\frac{\partial}{\partial y}(y\rho vv) = -y\frac{\partial p}{\partial y} + \frac{2}{Re_\infty}\left[y\frac{\partial \tau_{xy}}{\partial x}+\frac{\partial(y\tau_{yy})}{\partial y}-\tau_{\phi\phi}\right] \tag{3}$$

where

$$\tau_{xx} = 2\mu(\partial u/\partial x)-\tfrac{2}{3}\mu[(1/y)\,\partial(yv)/\partial y+\partial u/\partial x] \tag{4}$$

$$\tau_{xy} = \tau_{yx} = \mu[\partial u/\partial y+\partial v/\partial x] \tag{5}$$

$$\tau_{\phi\phi} = 2\mu(v/y)-\tfrac{2}{3}\mu[(1/y)\,\partial(yv)/\partial y+\partial u/\partial x] \tag{6}$$

$$\tau_{yy} = 2\mu(\partial v/\partial y)-\tfrac{2}{3}\mu[(1/y)\,\partial(yv)/\partial y+\partial u/\partial x] \tag{7}$$

The energy equation

Neglecting the compression work and viscous dissipation, the energy equation can be written as

$$\frac{\partial}{\partial x}(y\rho uh)+\frac{\partial}{\partial y}(y\rho vh) = \frac{2}{Pe_\infty}\left[\frac{\partial}{\partial x}\left(yk\frac{\partial T}{\partial x}\right)+\frac{\partial}{\partial y}\left(yk\frac{\partial T}{\partial y}\right)\right]. \tag{8}$$

With constant heat capacity, the enthalpy h is related to temperature T as $h = C_pT$ and the energy equation can be rewritten as

$$\frac{\partial}{\partial x}(y\rho uT)+\frac{\partial}{\partial y}(y\rho vT) = \frac{2}{Pe_\infty}\left[\frac{\partial}{\partial x}\left(y\frac{k}{C_p}\frac{\partial T}{\partial x}\right)+\frac{\partial}{\partial y}\left(y\frac{k}{C_p}\frac{\partial T}{\partial y}\right)\right] \tag{9}$$

The following dimensionless variables have been used for the above equations

$$u = u'/u'_\infty,\quad v = v'/u'_\infty,\quad T = T'/T'_\infty$$

$$p = p'/\rho'_\infty u'^2_\infty,\quad h = h'/c'_{p\infty}T'_\infty,\quad \rho = \rho'/\rho'_\infty$$

$$\mu = \mu'/\mu'_\infty,\quad C_p = C'_p/C'_{p\infty},\quad k = k'/k'_\infty$$

$$x = x'/R',\quad y = y'/R',\quad Re_\infty = 2R'u'_\infty\rho'_\infty/\mu'_\infty$$

$$Pr_\infty = C'_{p\infty}\mu'_\infty/k'_\infty,\quad Pe_\infty = Re_\infty\,Pr_\infty$$

The boundary conditions for multisphere cylindrical cell are

(a) at the inlet

$$u = 1, \quad v = 0, \quad T = 1\,;$$

(b) on the cylindrical envelope

$$u = 1, \quad \partial u/\partial y = 0, \quad v = 0, \quad T = 1\,;$$

(c) on the sphere surface

$$u = 0, \quad v = 0, \quad T = T_s,$$

(d) along the axis of symmetry

$$\partial u/\partial y = 0, \quad v = 0, \quad \partial T/\partial y = 0,$$

(e) at the outlet

u is adjusted to satisfy global mass conservation relation (see Apppendix), $v = 0$, $\partial T/\partial x = 0$.

The heat transfer to the sphere can be expressed in terms of the local or average Nusselt numbers

$$Nu_s = 2R'(k'_s/k'_\infty)(\partial T'/\partial r')_s/(T'_\infty - T'_s) \quad (10)$$

$$\overline{Nu} = 1/2 \int_0^\pi Nu_s \sin\theta \, d\theta \quad (11)$$

where r' and θ are radial and angular coordinates in spherical geometry The drag force acting on the sphere can be expressed in terms of the drag coefficients

$$C_{df} = \frac{8}{Re_\infty} \int_0^\pi (\tau_{r\theta} \sin\theta - \tau_{rr} \cos\theta) \sin\theta \, d\theta \quad (12)$$

where

$$\tau_{r\theta} = \mu \left[r \frac{\partial}{\partial r} \left(\frac{v_\theta}{r} \right) + \frac{1}{r} \frac{\partial v_r}{\partial \theta} \right] \quad (13)$$

$$\tau_{rr} = 2\mu \frac{\partial v_r}{\partial r} - \tfrac{2}{3}\mu \left[\frac{1}{r^2} \frac{\partial}{\partial r}(r^2 v_r) + \frac{1}{r \sin\theta} \frac{\partial}{\partial \theta}(v_\theta \sin\theta) \right] \quad (14)$$

$$v_r = u \cos\theta + v \sin\theta \quad (15)$$

$$v_\theta = u \sin\theta + v \cos\theta \quad (16)$$

$$C_{df} = 2 \int_0^\pi p_s \sin 2\theta \, d\theta. \quad (17)$$

The total drag is then

$$C_d = C_{df} + C_{dp} \quad (18)$$

In order to compare the present results with previously published data, a modified set of dimensionless groups, in which the fluid properties are evaluated at the film temperature, are defined as

$$Nu_f = 2R'(k'_s/k'_f)(\partial T'/\partial r')_s/(T'_\infty - T'_s) \quad (19)$$

$$Re_f = 2R' u'_\infty \rho'_\infty / \mu'_f \quad (20)$$

$$Pr_f = C'_p \mu'_f / k'_f \quad (21)$$

where the subscript f refers to the film temperature defined as

$$T'_f = (T'_s + T'_\infty)/2 \quad (22)$$

Transformation of the basic equations

The set of conservation equations can be written in a more general form for a general dependent variable as

$$\frac{\partial}{\partial x}(\rho y u \phi) + \frac{\partial}{\partial y}(\rho y v \phi) = \frac{\partial}{\partial x}\left(\Gamma y \frac{\partial \phi}{\partial x} \right) + \frac{\partial}{\partial y}\left(\Gamma y \frac{\partial \phi}{\partial y} \right) + Sy \quad (23)$$

For the axial velocity component (u) in the momentum equation

$$\phi = u, \quad \Gamma = \frac{2\mu}{Re_\infty},$$

$$\text{and} \quad S = -\partial p/\partial x + \text{viscous terms} \quad (24)$$

for the radial velocity component (v)

$$\phi = v, \quad \Gamma = \frac{2\mu}{Re_\infty},$$

$$\text{and} \quad S = -\partial p/\partial y + \text{viscous terms} \quad (25)$$

and for the energy equation

$$\phi = T, \quad \Gamma = \frac{2k}{Pe_\infty C_p}, \quad \text{and} \quad S = 0 \quad (26)$$

When new independent variables ξ and η are introduced, the partial derivatives of the function ϕ are transformed according to

$$\phi_x = (y_\eta \phi_\xi - y_\xi \phi_\eta)/J, \quad \phi_y = (-x_\eta \phi_\xi + x_\xi \phi_\eta)/J \quad (27)$$

where J is the Jacobian of the transformation given by $J = x_\xi y_\eta - x_\eta y_\xi$ By defining the following functions

$$G_1 = u y_\eta - v x_\eta \quad (28a)$$

$$G_2 = v x_\xi - u y_\xi \quad (28b)$$

$$\alpha = x_\eta^2 + y_\eta^2, \quad \beta = x_\xi x_\eta + y_\xi y_\eta, \quad \gamma = x_\xi^2 + y_\xi^2 \quad (29)$$

one can reduce equation (23) to

$$\frac{\partial}{\partial \xi}(\rho y G_1 \phi) + \frac{\partial}{\partial \eta}(\rho y G_2 \phi) = \frac{\partial}{\partial \xi}[(\Gamma y/J)(\alpha \phi_\xi - \beta \phi_\eta)] + \frac{\partial}{\partial \eta}[(\Gamma y/J)(\gamma \phi_\eta - \beta \phi_\xi)] + SyJ \quad (30)$$

Integration over the control volume and application of Green's theorem allows equation (30) to be written in integral form as

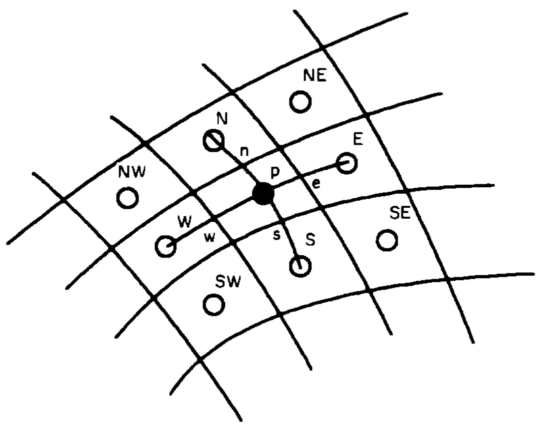

FIG 3(a). Finite-difference grid representation in the physical plane

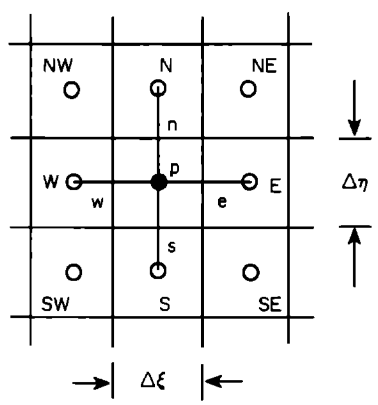

FIG 3(b) Finite-difference grid representation in the transformed plane

$$\int_B (\rho y G_1 \phi\, d\eta - \rho y G_2 \phi\, d\xi) = \int_B [(\Gamma y/J)(\alpha\phi_\xi - \beta\phi_\eta)\, d\eta - (\Gamma y/J)(\gamma\phi_\eta - \beta\phi_\xi)\, d\xi] + \iint_R SyJ\, d\xi\, d\eta. \quad (31)$$

With the notation shown in Fig. 3 for a typical grid node p enclosed in its cell and surrounded by its neighboring nodes N, S, E, and W, the finite-difference approximation of equation (31) over the cell can be written as

$$(\rho y G_1 \phi \Delta\eta)_w^e + (\rho y G_2 \phi \Delta\xi)_s^n = [(\Gamma y/J)(\alpha\phi_\xi - \beta\phi_\eta)\Delta\eta]_w^e + [(\Gamma y/J)(\gamma\phi_\eta - \beta\phi_\xi)\Delta\xi]_s^n + SyJ\Delta\xi\Delta\eta. \quad (32)$$

If the power law scheme [8] is used to evaluate the strength of convection and diffusion on the cell boundary, equation (32) can be recast as a relation between the value of ϕ at node p and its values at the neighboring nodes, i.e

$$A_p\phi_p = A_E\phi_E + A_W\phi_W + A_N\phi_N + A_S\phi_S + SyJ\Delta\xi\Delta\eta - [(\Gamma y/J)\beta\phi_\eta\Delta\eta]_w^e + [(\Gamma y/J)\beta\phi_\xi\Delta\xi]_s^n \quad (33)$$

where $A_p = A_E + A_W + A_N + A_S$ and the coefficients A_i (i = E, W, N, S) involve the convective flow parameters such as mass fluxes, areas, viscosities, diffusion coefficients, and the like. The details can be found in ref [8]. The terms within the brackets in equation (33) result from the non-orthogonal grid system They can be evaluated through the finite-difference approximation

$$[(\Gamma y/J)\beta\phi_\eta\Delta\eta]_e = 1/4[(\Gamma y/J)\beta\Delta\eta]_e(\phi_{NE} - \phi_{SE} + \phi_N - \phi_S) \quad (34)$$

Pressure equation

In the momentum equations, the pressure remains unknown. However, an independent equation for pressure can be set up by combining the continuity and momentum equations The details of the procedure will be described later in this section

The disadvantage of using the pressure/velocity formulation, as compared to the stream function/vorticity formulation, is that checkerboard pressure and velocity fields may result [8] Such unrealistic fields are linked to the use of central difference equations to express the first-order derivatives of pressure in the momentum equations and velocity in the continuity equation. The most common way to avoid these checkerboard fields is to use a staggered grid [8] For a curvilinear grid, however, a staggered grid can be overwhelmingly complicated.

There are a number of numerical schemes available, such as SIMPLE (Semi Implicit Method for Pressure Linked Equations [9]), SIMPLER (SIMPLE-Revised [10]), or SIMPLEM (SIMPLE-Modified [10]), that can be used to solve the equations for pressure and momentum These numerical schemes can avoid checkerboard pressure and velocity fields without adopting a staggered grid In the present analysis, SIMPLEM is adopted because of its good convergence characteristics, and the pressure equation is formulated accordingly The procedure and the strategy of SIMPLEM will be discussed briefly in the next section The pressure equation is derived by writing the momentum equations in the following form.

$$u = u^* + B_1(y\,\partial P/\partial\xi) + C_1(y\,\partial P/\partial\eta) \quad (35)$$

$$v = v^* + B_2(y\,\partial P/\partial\xi) + C_2(y\,\partial P/\partial\eta) \quad (36)$$

where

$$\begin{aligned} u^* &= \sum_{EWNS} A^u u + S^u, & v^* &= \sum_{EWNS} A^v v + S^v \\ B_1 &= -y_\eta\Delta\xi\Delta\eta/A_p^u, & C_1 &= y_\xi\Delta\xi\Delta\eta/A_p^u \\ B_2 &= x_\eta\Delta\xi\Delta\eta/A_p^v, & C_2 &= -x_\xi\Delta\xi\Delta\eta/A_p^v \\ A^u &= A_i^u/A_p^u, & A^v &= A_i^v/A_p^v \\ & & i &= \text{E, W, N, S} \end{aligned} \quad (37)$$

and S^u and S^v are residues after the pressure gradient terms have been extracted

Integration of the continuity equation (equation (1)) over the control volume yields

$$(\rho G_1 y\Delta\eta)_e-(\rho G_1 y\Delta\eta)_w+(\rho G_2 y\Delta\xi)_n-(\rho G_2 y\Delta\xi)_s=0 \quad (38)$$

With the above definitions of u and v, G_1 and G_2 can be written as follows

$$G_1=G_1^*+(B_1 y_\eta-B_2 x_\eta)(y\,\partial P/\partial\xi)+(C_1 y_\eta-C_2 x_\eta)(y\,\partial P/\partial\eta) \quad (39a)$$

$$G_2=G_2^*+(C_2 x_\xi-C_1 y_\xi)(y\,\partial P/\partial\eta)+(B_2 x_\xi-B_1 y_\xi)(y\,\partial P/\partial\xi) \quad (39b)$$

where

$$G_1^*=u^* y_\eta-v^* x_\eta \quad (40a)$$

$$G_2^*=v^* x_\xi-u^* y_\xi. \quad (40b)$$

With the substitution of G_1 and G_2 in the continuity equation (equation (38)), the pressure equation can be written as the algebraic equation

$$a_p p_p=a_E p_E+a_W p_W+a_N p_N+a_S p_S+b \quad (41)$$

where

$$\begin{aligned}
a_E &= (\rho y^2 B)_e(\Delta\eta/\delta\xi)_e\\
a_W &= -(\rho y^2 B)_w(\Delta\eta/\delta\xi)_w\\
a_N &= -(\rho y^2 C)_n(\Delta\xi/\delta\eta)_n\\
a_S &= -(\rho y^2 C)_s(\Delta\xi/\delta\eta)_s\\
a_p &= a_E+a_N+a_W+a_S\\
b &= (\rho G_1^* y\Delta\eta)_w-(\rho G_1^* y\Delta\eta)_e+(\rho G_2^* y\Delta\xi)_s\\
&\quad -(\rho G_2^* y\Delta\xi)_n+b_{no}\\
B &= B_1\,\partial y/\partial\eta-B_2\,\partial x/\partial\eta\\
C &= C_2\,\partial x/\partial\xi-C_1\,\partial y/\partial\xi
\end{aligned} \quad (42)$$

In the above equation b_{no} is the contribution due to nonorthogonality. It is expressed as

$$\begin{aligned}
b_{no} &= [(C_1 y_\eta-C_2 x_\eta)(y^2\,\partial P/\partial\eta)]_w\\
&\quad -[(C_1 y_\eta-C_2 x_\eta)(y^2\,\partial P/\partial\eta)]_e\\
&\quad +[(B_2 x_\xi-B_1 y_\xi)(y^2\,\partial P/\partial\xi)]_s\\
&\quad -[(B_2 x_\xi-B_1 y_\xi)(y^2\,\partial P/\partial\xi)]_n
\end{aligned} \quad (43)$$

Solution procedure

The numerical scheme SIMPLEM was used to solve the momentum and continuity equations The procedure of SIMPLEM, together with the solution procedure of solving the coupled energy equation, can be summarized as follows

(1) Start with assumed values for the fields u, v, P and T

(2) Calculate the coefficients of the momentum equations and u^* and v^* Use these values to find G_1^* and G_2^* at grid nodes Interpolate linearly to find G_1^* and G_2^* at the control volume faces

(3) Calculate the coefficients of the pressure equation and solve it to obtain a new pressure field

(4) Update G_1 and G_2 (equation (39)) at the interfaces using the new pressure field, and using $1-\Delta\xi$ or $1-\Delta\eta$ centered difference scheme for p

(5) Use the updated G_1 and G_2 to recalculate the coefficients of the momentum equation and use the new pressure field (obtained in step 2) to calculate the pressure gradient in the momentum equation with a $2-\Delta\xi$ or $2-\Delta\eta$ centered difference scheme The momentum equation can then be solved to obtain a new velocity field, i.e new u and v

(6) With the new velocity field, calculate the coefficients of the energy equation and solve it to obtain a new temperature field

(7) Use the calculated u, v, P and T as the new guess, return to step 2, and repeat until a converged solution is achieved

The purpose of using a centered $1-\Delta\xi$ or $1-\Delta\eta$ pressure difference scheme in step 4 is to detect any oscillation occurring in the flow field, and to suppress it immediately with the interface velocity The recalculation of the coefficients of the momentum equation in step 5, after updating the interface velocities, is to ensure that velocities used in the coefficients and the pressure field satisfy the same continuity equation. A more detailed discussion of the SIMPLEM procedures can be found in ref. [10] A standard tri-diagonal matrix algorithm (TDMA) is used to solve for the pressure equation in step 2, the velocity equation in step 5, and the temperature equation in step 6 The details of TDMA can be found in ref [8]

The grid system

The grid system used for the present analysis, as shown in Fig 2, is an embedded grid. Close to the sphere, a spherical grid is retained The remaining flow region is covered with a curvilinear mesh, which is generated by the method developed by Knight [11] This technique consists of solving Poisson's equation and performing an intermediate and final transformation The generated grid can be either orthogonal (with partial control of the mesh spacing) or nearly orthogonal (with full control of mesh spacing) In this work, we used the first of these options. Since orthogonality is not required for the curvilinear mesh, however, any other appropriate technique can be used to generate the mesh With this embedded grid, the computational domain can then be as shown in Fig 4(a) Figures 4(b) and (c) show the transformed calculation domain and the boundaries (meshed area) for the curvilinear mesh and spherical mesh, respectively The calculations are carried out in each of the two domains at each iteration, first in the curvilinear mesh and then in the spherical mesh It can be seen from Fig 4(b) that one row of the interior nodes in the spherical mesh serves as a boundary condition for the calculation in the curvilinear mesh. Figure 4(c) indicates how the intersection between the curvilinear mesh and the spherical mesh serves as a boundary condition when the calculation is performed in the

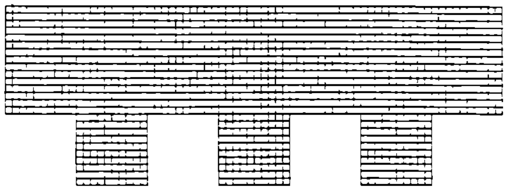

FIG 4(a) The computational plane for the entire embedded grid (Fig 2)

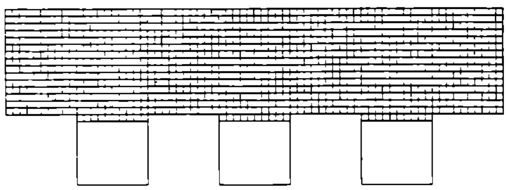

FIG 4(b) The computational plane for a curvilinear mesh (meshed area)

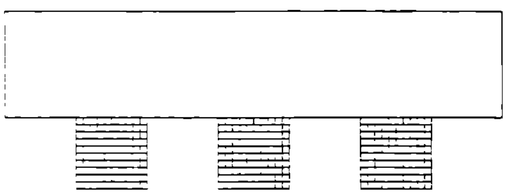

FIG 4(c) The computational plane for a spherical mesh (meshed area)

spherical mesh. It should be mentioned that the slab corners in the transformed domain are points which require special treatment. In this study the values at the special points were obtained by linear interpolation between the neighboring nodes along the axis of symmetry in the physical domain; a linear distribution of partial derivatives in the neighborhood of a special point was assumed Other techniques for treating the special point can be found in ref. [12].

RESULTS AND DISCUSSION

Calculations were first carried out for a single, isolated sphere immersed in flowing air. Experimental and numerical data for this case are abundant [13]. For these calculations, all the data, as well as the transport coefficients and thermodynamic properties are taken directly from the work of Renksizbulut and Yuen [13] in order to compare the present results with their results. The sphere temperature, air temperature, and Prandtl number (based on free stream properties) were taken as 353 K, 800 K, and 0.689, respectively The transport coefficients for air were approximated by $\mu = T^{0.67}$ and $k = T^{0.81}$ The air density varied with temperature as $\rho = 1/T$ and the heat capacity was taken as $C_p = 1$. The envelope of the multisphere cylindrical cell was set at 12 radii away from the axis of symmetry to ensure zero gradients on the envelope The inlet and outlet of the cell were kept at a distance of about 8 radii from the spheres

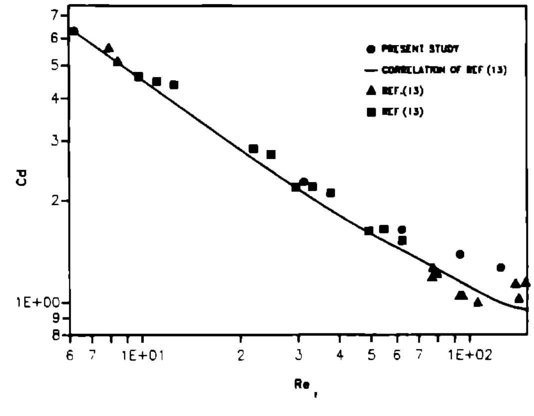

FIG 5 Drag coefficient for an isolated solid sphere

The criterion of convergence between two successive iterations was originally set at 10^{-4} in order to conserve computer time. However, it was found that the resulting dependence of average Nusselt number on Reynolds number was not smooth and tended to oscillate. This same phenomenon has also been reported by Aminzadeh *et al.* [4]. Therefore, a criterion of convergence of 10^{-5} was used and good results were obtained A relaxation factor of 0.8 was used for the calculation at Reynolds numbers below 50, while for Reynolds numbers greater than 50, a relaxation factor of 0.6 was used

The calculated drag coefficients and average Nusselt numbers of the isolated solid sphere are compared with the numerical results of Renksizbulut and Yuen [13] in Figs 5 and 6. Note that here the Reynolds number and the average Nusselt number are evaluated at the film temperature The agreement between the present results and the results of ref [13] is very good. Since the numerical results in ref. [13] correlate with a wide range of experimental data, the present results are also in good agreement This favorable comparison validates the present analysis and the numerical procedure, and justifies extending the calculations to a multisphere system

Numerical solutions have been obtained for three-sphere arrays with sphere spacings of 4 and 8 radii,

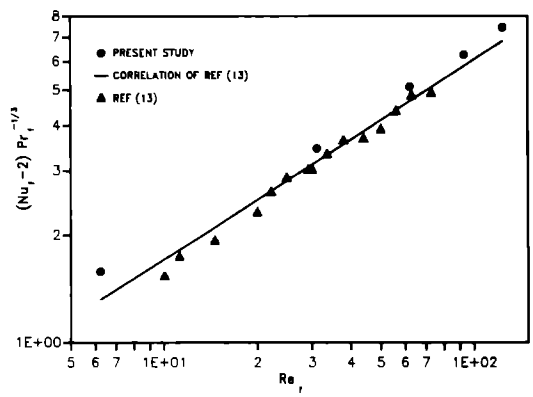

FIG 6 Numerical heat transfer data for an isolated solid sphere

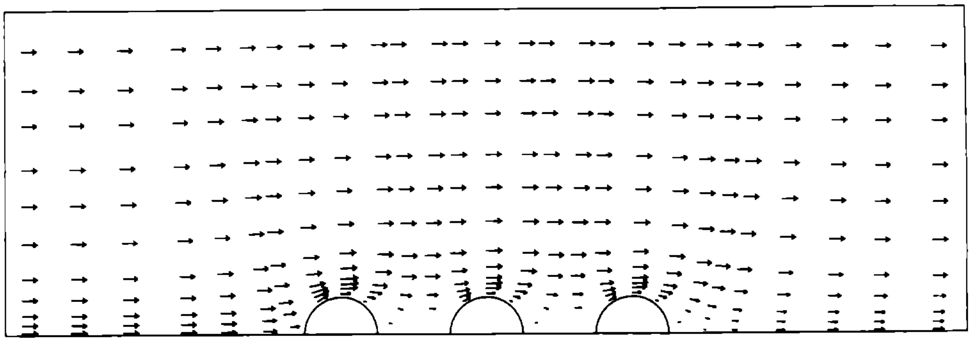

FIG 7(a) Velocity field in the entire cylindrical cell for a three-sphere array at $Re = 100$ and $L/R = 4.0$

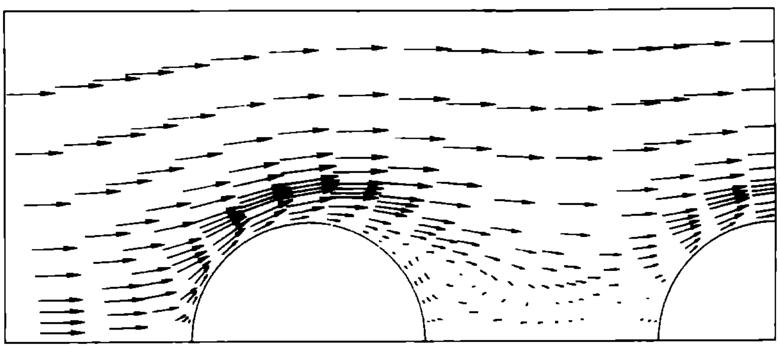

FIG 7(b) Velocity field around the first and the second spheres

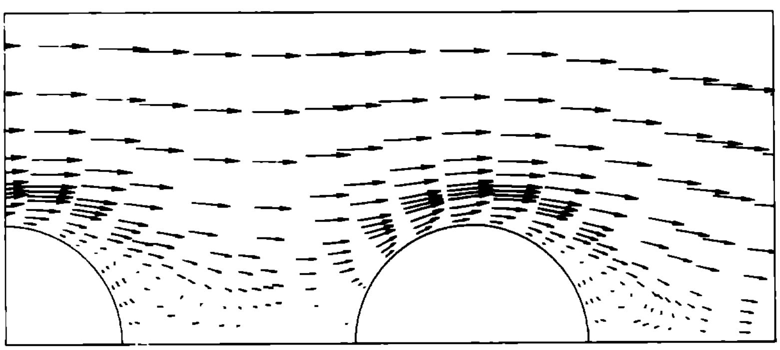

FIG 7(c) Velocity field around the second and the third spheres

and an array with spheres of three different sizes. The calculations were performed in a mesh consisting of a 150×42 grid plus three spherical meshes with 21×11 grids (see Fig 2) and the CPU time requirement is typically about 30 min in a Floating Point System (FPS) 264 to reach converged solutions for most cases discussed below For a sphere array with spacing of 4 radii, the flow field and the isotherm pattern at $Re = 100$ can be seen in Figs 7(a)–(c) and 8(a). In Figs 7(b) and (c), it can be seen that the second and third spheres clearly interact with the wake of the first and second spheres, respectively

In Fig. 8(a), very similar isotherm patterns can be observed among these three spheres, however, these patterns are not periodic. Figure 8(b) shows the isotherms of the three-droplet array with spacing of 8 radii at $Re = 100$ As can be seen in Fig 8(b), a periodic behavior emerges for the isotherm pattern of the second and third sphere This periodic behavior was not observed in Tal *et al*'s work [6], and the discrepancy might be due to the shorter spacings (3 and 6 radii) used in their study For comparison, the isotherms for the array with three different sizes of spheres at $Re = 50$ are also presented here and shown in Fig 8(c)

Figures 9(a) and (b) show the local Nusselt number for each of three spheres with a spacing of 4 and 8 radii at Reynolds numbers of 100. It is interesting to note in Fig. 9(a) that the wake behind the spheres at $Re = 100$ tends to increase the Nusselt number in the region after the polar angle of 140 (measured from the front stagnation point) The local Nusselt numbers of

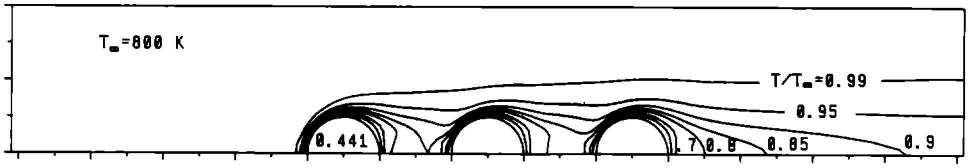

FIG 8(a) Isotherm pattern for three spheres at $Re = 100$ and $L/R = 4.0$

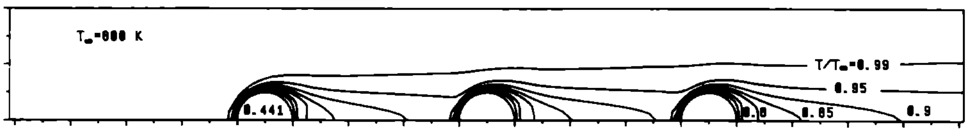

FIG 8(b) Isotherm pattern for three spheres at $Re = 100$ and $L/R = 8.0$

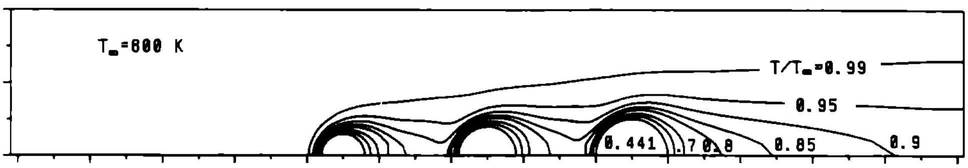

FIG 8(c) Isotherm pattern for three different-size spheres at $Re = 50$ and $L/R = 4.0$

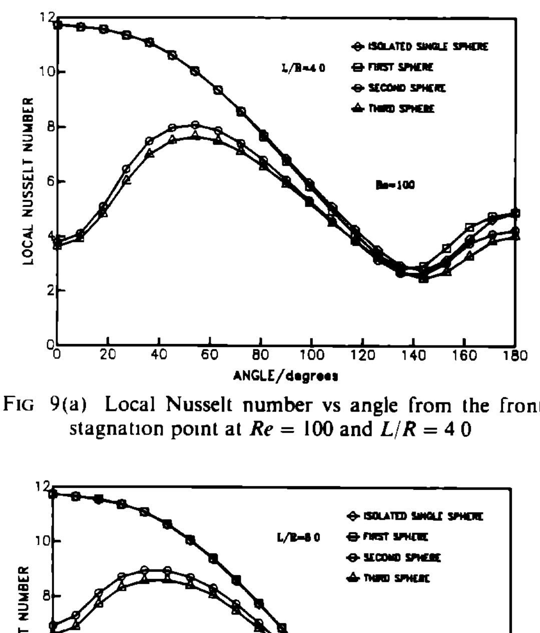

FIG 9(a) Local Nusselt number vs angle from the front stagnation point at $Re = 100$ and $L/R = 4.0$

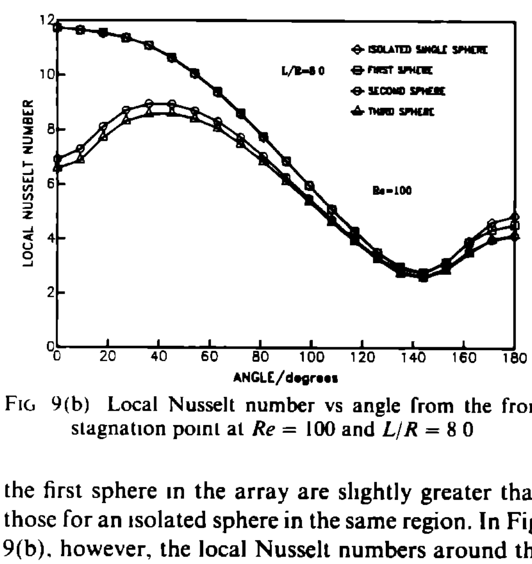

FIG 9(b) Local Nusselt number vs angle from the front stagnation point at $Re = 100$ and $L/R = 8.0$

the first sphere in the array are slightly greater than those for an isolated sphere in the same region. In Fig. 9(b), however, the local Nusselt numbers around the first sphere are the same as that of a single, isolated sphere This indicates that the heat transfer of the first sphere is not influenced by the presence of the downstream spheres Comparison of Figs. 9(a) and (b) shows that the local Nusselt numbers for the second and third spheres, at larger spacing, are higher than those for the same spheres at smaller spacing, which shows the sphere–sphere interaction decreases as the spacing between the spheres increases

The result of the overall average Nusselt number and total drag coefficient at a sphere spacing of 4 and 8 radii as a function of Reynolds number are shown in Figs. 10 and 11, respectively These results confirm the local variations discussed above Particularly, it can be observed that when the sphere spacing is increased, the difference of the average Nusselt number and the total drag coefficient between the first sphere and the rest of the spheres is reduced, i e. the interaction is reduced The value of the Nusselt number and total drag coefficient is higher for the first

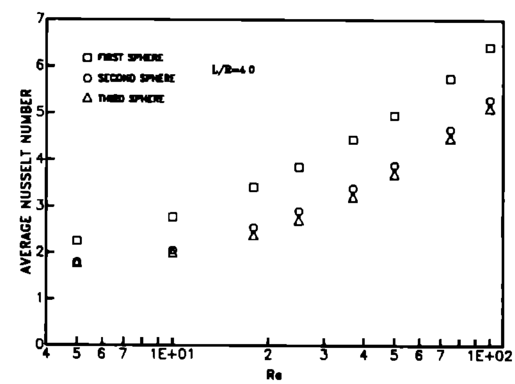

FIG 10(a) The average Nusselt number vs Reynolds number at $L/R = 4.0$

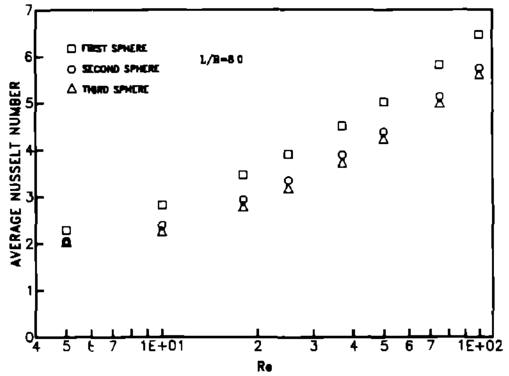

FIG 10(b) The average Nusselt number vs Reynolds number at $L/R = 8\ 0$

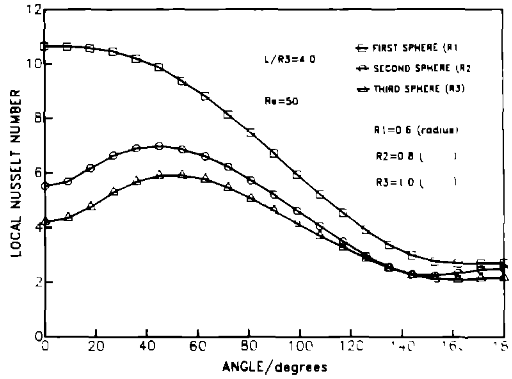

FIG 12 Local Nusselt number vs angle from the front stagnation point for three different-size spheres at $Re = 50$ and $L/R = 4\ 0$

sphere, and the values for the second and the third spheres are nearly the same This agrees with the results reported by Chen and Tong [5] and Tal *et al* [6]

The local Nusselt numbers for three spheres with different sizes and equal size at $Re = 50$ are shown in Figs. 12 and 13, respectively. In Fig. 12, the radius of the largest sphere (third sphere) is used as the characteristic length for the local Nusselt number and Reynolds number. It can be observed that the smallest sphere (first sphere) has the highest heat transfer rate on the sphere surface Comparison between Figs. 12 and 13 indicates that the small upstream spheres give less influence on the heat transfer of the downstream spheres

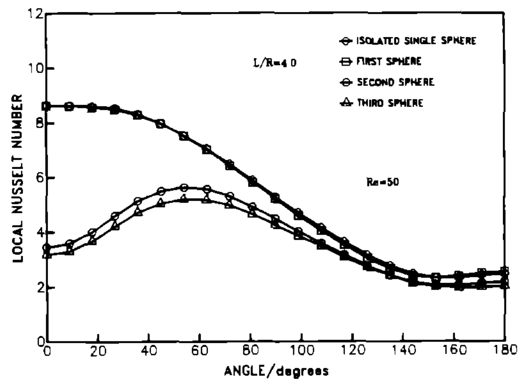

FIG 13 Local Nusselt number vs angle from the front stagnation point for three equal-size spheres at $Re = 50$ and $L/R = 4\ 0$

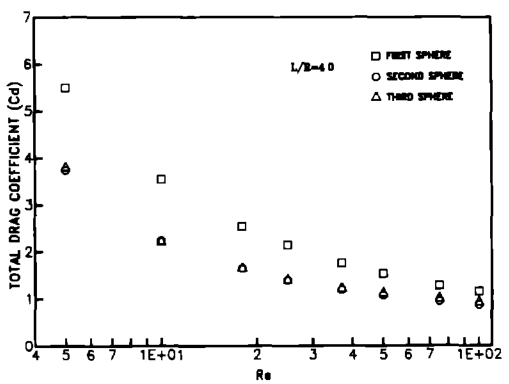

FIG 11(a) Total drag coefficient vs Reynolds number at $L/R = 4\ 0$

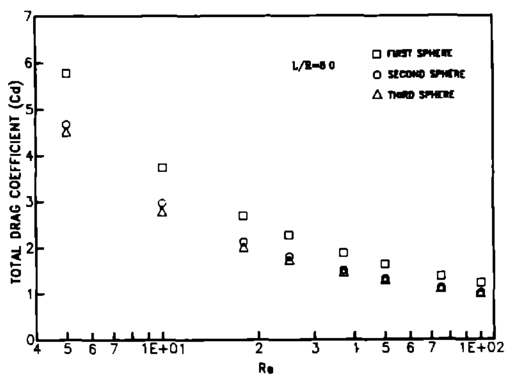

FIG 11(b) Total drag coefficient vs Reynolds number at $L/R = 8\ 0$

CONCLUSIONS

A numerical scheme, SIMPLEM, and an embedded, body fitted grid are used to obtain the solution of heat and momentum transfer in one-dimensional sphere arrays for Reynolds numbers from 5 to 100. The following conclusions can be drawn from this analysis

(1) The present numerical scheme has been applied to a single, isolated sphere and the results show good agreement with the available numerical results and experimental data

(2) The calculations in the present analysis are based on variable gas properties Since most practical heat transfer problems involve large property variations, the present study appears to be more relevant than those where constant properties are assumed

(3) The interaction between equal-size spheres is found to decrease as the sphere spacing increases For spheres with different sizes, it is also found that a small sphere tends to have a higher heat transfer rate and less influence on the heat transfer of the downstream spheres

(4) The velocity–pressure form used for the momentum equation in the present study could be more easily extended to three-dimensional problems than the stream function/vorticity form used in most other related analyses reported in the literature.

(5) For linear droplet arrays undergoing combustion, the present heat transfer analysis, when coupled with the species conservation equations, can be used to calculate the burning rate of linear droplet arrays. This analysis is currently in progress and the results will be reported in future communications

Acknowledgement—This work has been funded, in part, by the United States Environmental Protection Agency through Cooperative Agreement No CR809714010 granted to the Hazardous Waste Research Center of Louisiana State University Although this research has been supported by the USEPA, it has not been subjected to Agency review and therefore does not necessarily reflect the views of the Agency and no official endorsement should be inferred

REFERENCES

1 A Umemura, S Ogawa and N Oshima, Analysis of the interaction between two burning fuel droplets with different sizes, *Combust Flame* **43**, 111–119 (1981)
2 M Labowsky, Calculation of the burning rates of interacting fuel droplets, *Combust Sci Technol* **22**, 217–226 (1980)
3 J S Shuen, Effect of droplet interactions on droplet transport at intermediate Reynolds numbers, AIAA 25th Aerospace Sciences Meeting, Reno, Nevada (1987)
4 K Aminzadeh, T R Al Taha, A R H Cornish, M S Kolansky and R Pfeffer, Mass transport around two spheres at low Reynolds numbers, *Int J. Heat Mass Transfer* **17**, 1426–1436 (1974)
5 S J Chen and A. Y Tong, Application of elliptic grid generation technique to the solution of hydrodynamics and heat transfer of droplet arrays at intermediate Reynolds numbers, *Int J Heat Mass Transfer* **31**, 1063–1072 (1988)
6 R Tal, D N Lee and W A Sirignano, Hydrodynamics and heat transfer in sphere assemblages multisphere cylindrical cell models, AIAA 20th Aerospace Sciences Meeting, Orlando, Florida (1982)
7 R Tal, D N Lee and W A Sirignano, Heat and momentum transfer around a pair of spheres in viscous flow, *Int J Heat Mass Transfer* **27**, 1953–1962 (1984)
8 S V Patankar, *Numerical Heat Transfer and Fluid Flow* McGraw-Hill, New York (1981)
9 C M Rhie and W L Chow, Numerical study of the turbulent flow past an airfoil with trailing edge separation, *AIAA J* **21**(11), 1525–1532 (1983)
10 F H Moukalled, Adaptive grid solution procedure for elliptic flow, Ph D Dissertation, Louisiana State University, Baton Rouge, Louisiana (1987)
11 D D Knight, Application of curvilinear coordinate generation techniques to the computation of internal flows In *Numerical Grid Generation* (Edited by J F Thompson) Elsevier Science, Amsterdam (1982)
12 J F Thompson, Z U A Warsi and C W Mastin, *Numerical Grid Generation—Foundations and Applications* Elsevier, Amsterdam (1985)
13 M Renksizbulut and M C Yuen, Numerical study of droplet evaporation in a high-temperature stream, *J Heat Transfer* **105**, 389–397 (1983)

APPENDIX

The velocity component u at the outlet of the cylindrical cell is adjusted to satisfy mass conservation at each iteration as follows

The total mass flow rate (based on unit radian) into the cylindrical cell is calculated at the cell inlet as

$$Q = \sum_{j=1}^{M} \rho_j u_j \Delta Y_j Y_j$$

An estimate of the total outlet flow is calculated using the u component of velocity one node upstream of the exit as

$$\hat{Q} = \sum_{j=1}^{M} \rho_j^L u_j^{L-1} \Delta Y_j Y_j$$

The u component of velocity at the exit of the cylindrical cell is then adjusted by

$$u_j^L = u_j^{L-1}(Q/\hat{Q})$$

where j is the index of the node in the y-direction, M the largest number of j, $\Delta Y_j Y_j$ the flow area associated with node j, L the index of outlet, $L-1$ the index of the interior nodes one node upstream from the outlet, and $Q(\hat{Q})$ the actual (estimated) mass flow rate

APPLICATION DE LA GRILLE NOYEE A LA RESOLUTION DU TRANSFERT DE CHALEUR ET DE QUANTITE DE MOUVEMENT POUR DES SPHERES EN ARRANGEMENT LINEAIRE

Résumé—L'objectif de cette étude est de prédire le transfert thermique par convection forcée pour des sphères dans un arrangement monodimensionnel aligné dans la direction de l'écoulement Un arrangement avec des sphères de diamètres différents est aussi étudié L'interaction de ces sphères est le fait marquant de l'analyse Les équations de Navier–Stokes, sous la forme pression–vitesse et l'équation d'énergie sont résolues numériquement par une méthode itérative aux différences finies dans une grille noyée. On étudie le domaine de nombre de Reynolds de 5 à 100 pour deux espacements des sphères La distribution de température autour des sphères et le coefficient de trainée sont calculés ainsi que le nombre de Nusselt autour des sphères Les résultats montrent un bon accord avec ceux numériques et expérimentaux de la littérature

ANWENDUNG EINES FESTEN GITTERS ZUR LÖSUNG DES WÄRME- UND IMPULSTRANSPORTS FÜR KUGELN IN EINEM LINEAREN FELD

Zusammenfassung—Ziel dieser Untersuchung ist die Berechnung des Warmetransports in erzwungener Stromung in einem Feld von Kugeln, welche hintereinander angeordnet sind Neben gleichen Kugeln wurde auch ein Feld mit Kugeln unterschiedlicher Große betrachtet Die gegenseitige Beeinflussung der Kugeln ist ein wesentlicher Gesichtspukt der Untersuchung Die Navier–Stokes-Gleichungen (in Druck-Geschwindigkeitsform) und die Energiegleichung werden numerisch mit Hilfe einer iterativen Finite-Differenzen-Methode gelost Dabei wird ein feststehendes, an den Kugeln zentriertes Gitter benutzt Die Untersuchungen werden fur zwei verschiedene Kugelabstande und Reynolds-Zahlen im Bereich von 5–100 durchgefuhrt Es wird sowohl die Temperaturverteilung in der Umgebung des Kugelfeldes als auch der Widerstandsbeiwert und die Nusselt-Zahlen an den Kugeloberflachen berechnet Die Ergebnisse zeigen eine gute Ubereinstimmung mit numerischen und experimentellen Ergebnissen aus der Literatur

ПРИМЕНЕНИЕ МЕТОДА СЕТОК ДЛЯ РЕШЕНИЯ ЗАДАЧ ПЕРЕНОСА ТЕПЛА И ИМПУЛЬСА В ЛИНЕЙНОЙ ЦЕПОЧКЕ СФЕР

Аннотация—Целью данного исследования является предсказание теплопереноса вынужденной конвекции в одномерной цепочке сфер, расположенных в направлении течения. Рассматривается также случай цепочки сфер различных размеров. Особенностью анализа является взаимодействие между сферами Уравнения Навье–Стокса в координатах "скорость и давление", а также уравнение сохранения энергии решаются численно итерационным конечно–разностным методом Исследуется диапазон значений числа Рейнольдса 5–100 для двух промежутков между сферами. Рассчитываются распределение температуры вокруг цепочки сфер, а также коэффициент сопротивления и число Нуссельта вокруг их поверхностей. Полученные результаты хорошо согласуются с имеющимися в литературе численными и экспериментальными данными